

COMPTON COINCIDENCE MEASUREMENT

Albert H. Walenta^a, Kıvanç Nurdan^a and Tuba Çonka-Nurdan^a,

a) Department of Physics, Detector Physics and Electronics Group, University of Siegen, Siegen, Germany

Instructions for the Laboratory Course

*2nd ICFA Instrumentation School
ICFA Center İstanbul, 2005*

Introduction

If monochromatic X rays beam strikes a target, they may be absorbed (“photoeffect”) or scatter from both atomic nuclei and the surrounding electrons. Here we focus mainly on the scattering process. An electromagnetic wave may pass near an electron and excite it into oscillations at the same frequency and at the same phase as the incident photon. Scattering of the photons in this case is elastic(*coherent scattering*), so the measured spectrum of the scattered X rays shows a peak at the original wavelength. However, the scattering of X rays from individual atomic electrons is “inelastic”, where the photons loose some of their energy in this process. This phenomenon is called a “Compton Scattering”. The relative probability of Compton scattering ($\sigma \sim Z$) compared to coherent scattering ($\sigma \sim Z^2$) and photo-absorption ($\sigma \sim Z^5$) decreases with decreasing atomic number of the element.

At high γ -energy transfer, the energy of an atomic electron before scattering can be neglected in good approximation ($E_\gamma - E_\gamma' \gg E_B$, with E_B the binding energy). This is the Compton scattering at a quasi-free electron. In this case the electron can be considered as being at rest and E_γ' is a function of E_γ and the scattering angle only.

Thus the typical feature of the Compton scattering is the “particle picture” where the kinematics of the collision process can be calculated classically observing the relativistic forms of energy – and momentum conservation.

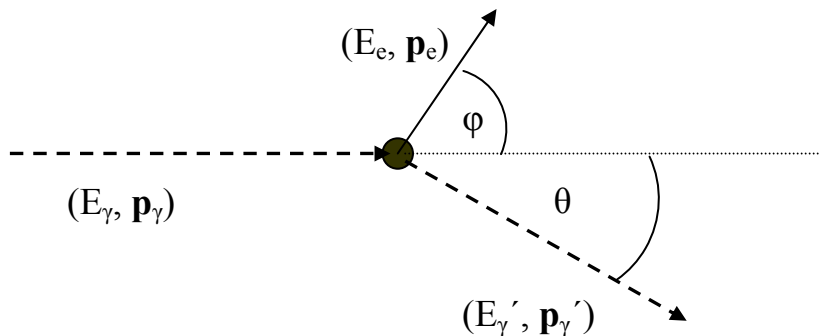


Fig. 1. Kinematics of Compton Scattering (schematically)

Under these conditions it is obtained (derivation see Appendix A):

$$E_\gamma' = E_\gamma \frac{1}{1 + \alpha(1 - \cos \theta)} \quad \text{with} \quad \alpha = \frac{E_\gamma}{m_e c^2} \quad \text{and} \quad m_e \text{ the electron rest mass.}$$

Since $E_\gamma = E_e + E_\gamma'$ for the electron energy it is obtained:

$$E_e = E_\gamma \frac{\alpha(1 - \cos \theta)}{1 + \alpha(1 - \cos \theta)}$$

Fig. 2 shows the energies of the scattered photon and the ejected electron as function of θ for an incoming γ -ray of 662 keV from a ^{137}Cs source as used in the experiment. It is noted that the maximum energy transferred to the electron is reached for a scattering angle $\theta = 180$ degrees.

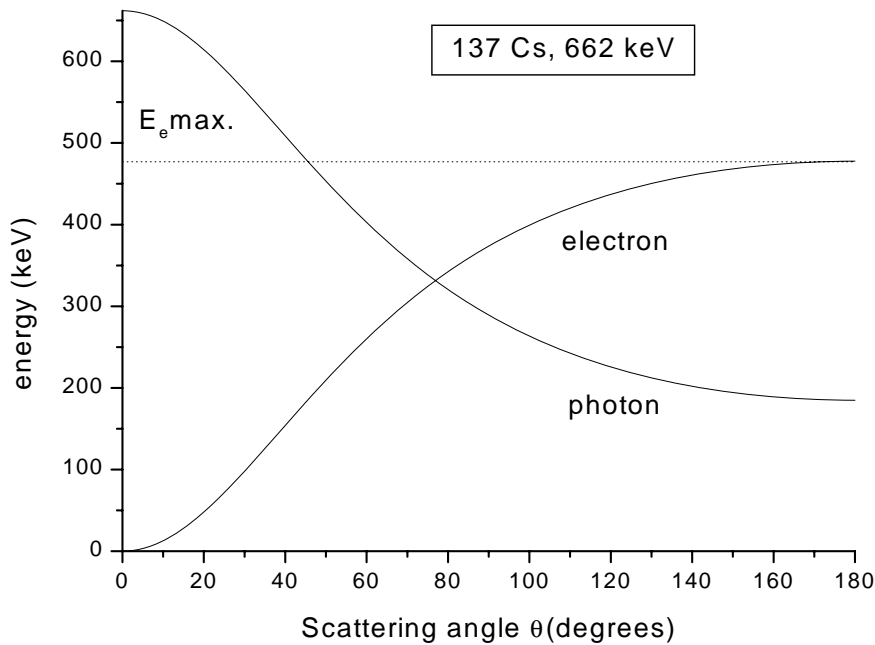


Fig. 2. Energy of scattered photon and ejected electron as function of scattering angle θ (see fig.1)

For an electron of the inner shell (e.g. K-shell) at high Z , the binding energy may become comparable to $E_\gamma - E_{\gamma'}$. This has to be taken into account for the calculation of the energy balance. In addition the momentum distribution of this bound electron cannot be neglected as well and leads to a significant broadening of the angular response for a given energy transfer.

The aim of this experiment is to observe and analyze Compton Scattering by using the coincidence of the pulses from a fixed plastic scintillation detector recording the ejected electron and a NaI(Tl) scintillator detector adjustable at different angles for recording the scattered photon. The experimental techniques involved are scintillators and photomultipliers as well as analogue and digital circuits.

Discovery of Compton Effect

The quantitative establishment of the Compton Effect (Fig. 3) in 1923 by Arthur Holy Compton was a crucial evidence in support of the corpuscular character of electromagnetic radiation.

In his experiment, a collimated beam of Molybdenum K_α X-rays were scattered from a Carbon target. The wavelength of the scattered X rays was measured by the technique of high-resolution X-ray spectrometry using X-ray diffraction from a crystal and applying Bragg's law. An ionization chamber was used as the detector in the spectrometer. According to the classical expectation, the wavelength of the scattered X rays would be the same as that of the incident X rays and only the intensity of them would depend on the angle θ through which the X-ray detection apparatus was

rotated. However, it is observed that there are two different spectral lines, one at a wavelength of the incident beam λ_0 and another at a wavelength $\lambda' > \lambda_0$ and the difference increased as θ increased (Fig. 4).

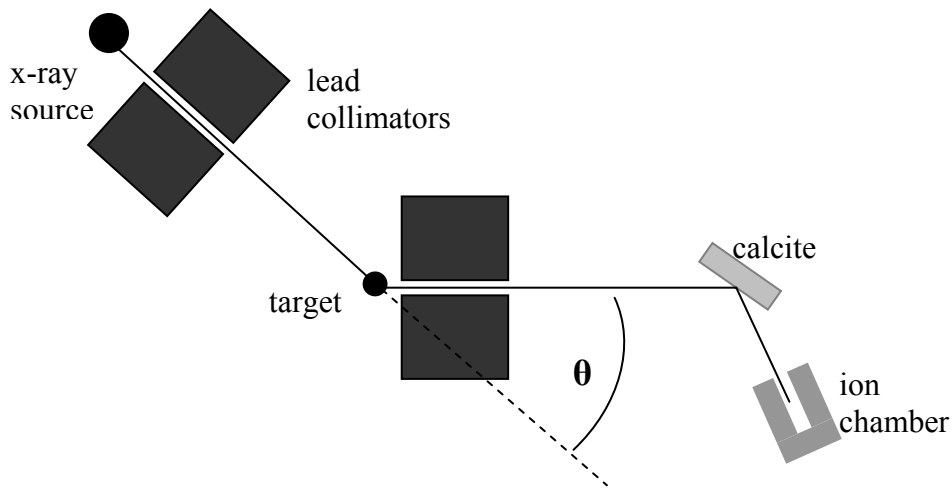


Fig. 3. Compton's Apparatus for the measurement of scattered photons.

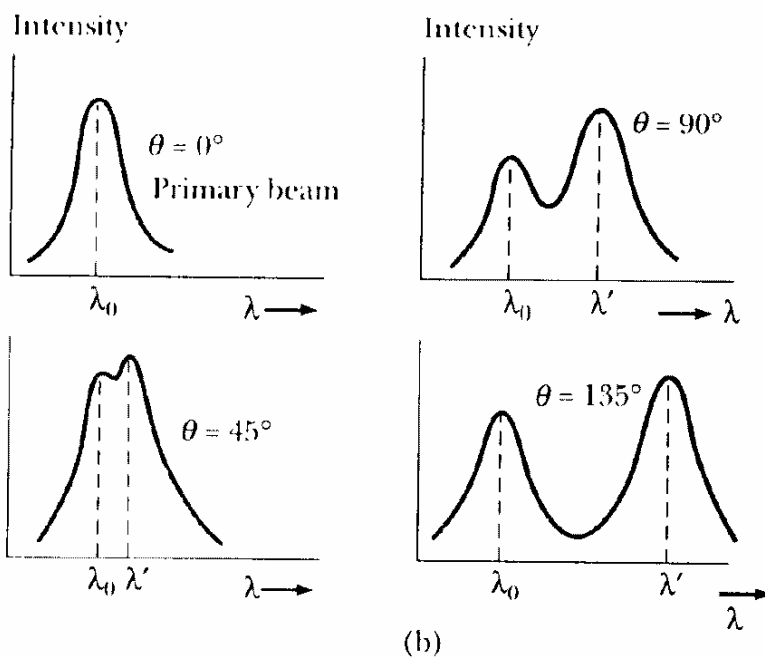


Fig. 4 Results of measurements with the apparatus of fig. 3

The classical theory had no explanation for the wavelength-shift, but with the modern concept of photon, acting like a particle carrying energy $E = h \nu$ and a momentum $p = h \nu/c$, it was easy to explain the situation. Compton could arrive at the formula for the *Compton Shift* in the wavelength of incoherently scattered X rays by assuming the scattering as a collision between a single photon and a single electron in which energy and momentum are conserved. The scattering formula is:

$$\lambda' - \lambda = \frac{h}{m_e c} (1 - \cos \theta) = \lambda_c (1 - \cos \theta)$$

where λ_c is the Compton wavelength of the electron and it is equal to 2426 fm.

At a time (early 1920's) when the particle (photon) nature of light suggested by the photoelectric effect was still being debated, the Compton experiment gave clear and independent evidence of particle-like behavior. The final evidence for this hypothesis was obtained by Compton when he observed the track of the ejected electron in a cloud chamber. An earlier experiment of Geiger and Bothe had shown that the scattered photon and the ejected electron came from the same scattering process. They applied for the first time the coincidence measurements using fast “Geiger” counters. It provided the confirmation of the validity of Planck's quantum hypothesis that electromagnetic radiation came in discrete mass-less packets with energy proportional to frequency. Compton was awarded the Nobel Prize in 1927 for the discovery of the effect named after him.

In 1929 Klein and Nishina calculated the angular distribution of the Compton scattering and this was one of the first applications of quantum electrodynamics(QED). The probability for a Compton scatter to occur at an angle θ can be calculated from the *Klein-Nishina* formula for the differential cross section per electron:

$$\frac{d\sigma_c}{d\Omega} = \frac{r_0^2}{2} \frac{1}{[1 + \alpha(1 - \cos \theta)]^2} \left[1 + \cos^2 \theta + \frac{\alpha^2 (1 - \cos \theta)^2}{1 + \alpha(1 - \cos \theta)} \right]$$

where α is the photon energy in units of the electron rest mass energy ($\alpha = E_\gamma/m_0c^2$) and r_0 is a parameter called the classical electron radius, which is equal to $r_0 = e^2/4\pi\epsilon_0 m_0 c^2 = 2.818$ fm.

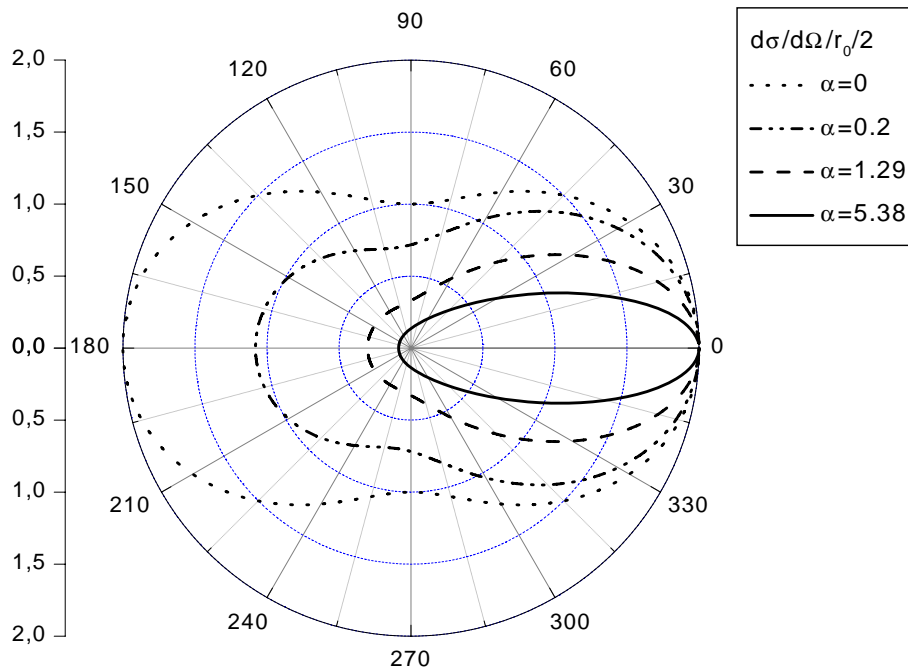


Fig. 5. Differential scattering given by the Klein Nishina formula in a polar diagram.

It is instructive to plot the Klein Nishina formula in polar coordinates where the radius is given by the differential cross section $d\sigma/d\Omega$ (Fig. 5). At low E_γ (or small α) the well known $1+\cos^2\theta$ distribution is obtained which progressively deformed in forward direction with increasing α .

Experimental Apparatus

Modern technology allows the direct verification of the Compton effect. The experimental arrangement is shown in Fig. 6. The setup consists of a γ source with a lead collimator and the detectors including read out electronics. The scatter detector is mounted on a support plate (plywood) such that it is placed at the center of a circle and the absorption detector can be moved to cover the angles -90 to $+90$ degrees and be fixed in positions in 15 degree intervals.

A ^{137}Cs radioactive source ($6 \mu\text{Ci}$) is used to provide the photons of $E_\gamma = 662 \text{ keV}$ for scattering. At this energy the effect is well observable. Another reason for the use of this source is the fact that the emission spectrum is mainly mono-energetic as can be seen from the decay schematics (Fig 1 in the Appendix B)

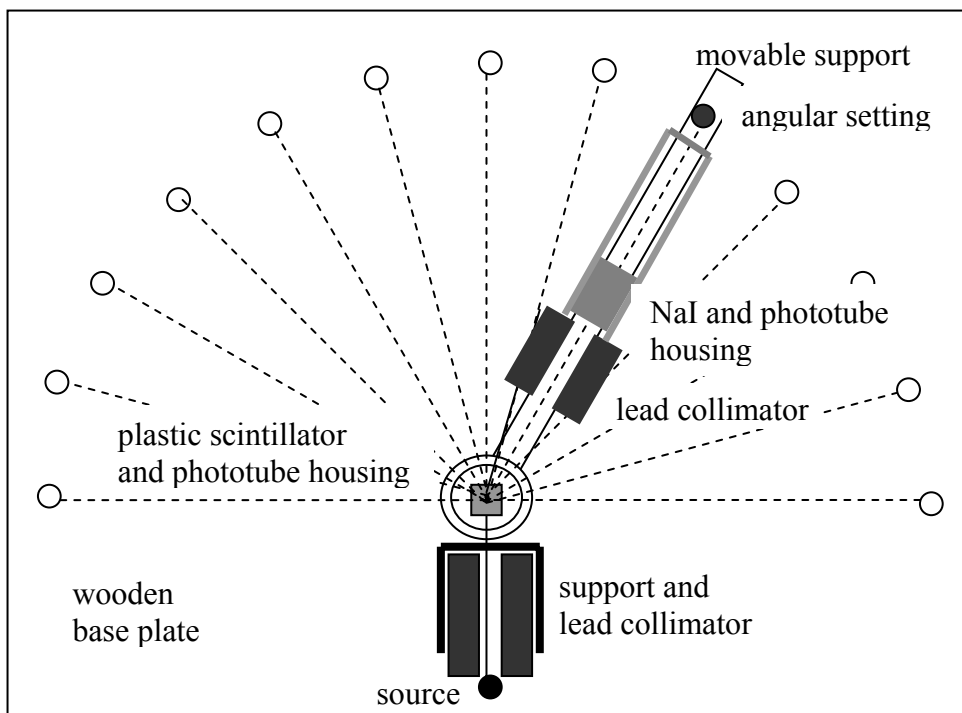


Fig. 6. Experimental set-up (top view)

The first detector uses a low Z plastic scintillator as active target. In this way the Compton electron is well detected and the pulse height is a measure of the energy while the scattered photon has a high chance to leave the material without further scattering. Fig. 7 shows the efficiency for a single interaction, the probability for a second interaction and the overall probability for all interactions in units of absorption length x_0 . For simplicity it has been assumed that the scattered photon has the same absorption length as the primary photon which is fulfilled since the cross section changes slowly in this energy regime (about 10%). Then it is obtained:

$$P_{\text{single}} = \frac{x}{x_0} e^{-x/x_0}$$

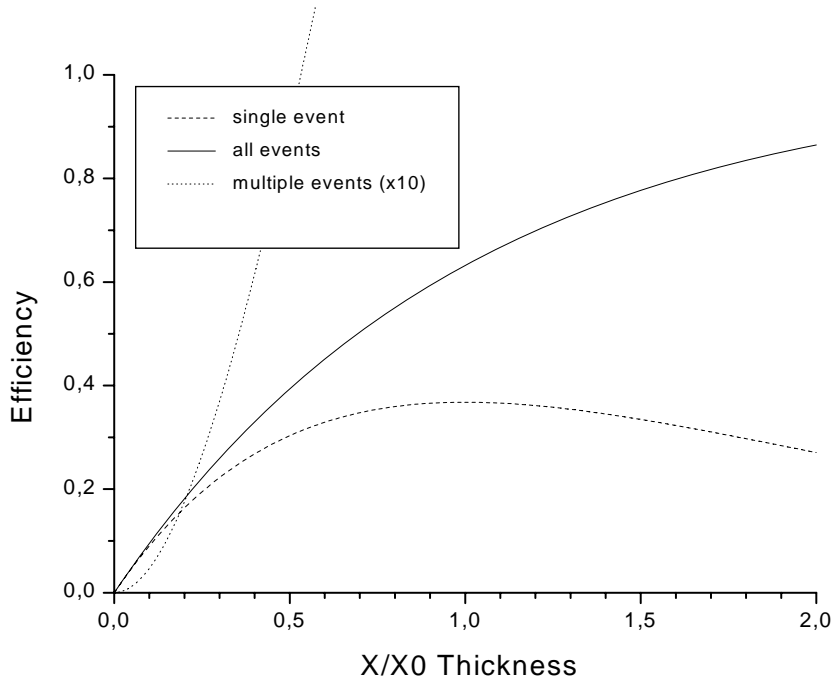


Fig. 7. Interaction probability in plastic scintillator material for $E_\gamma = 662 \text{ keV}$.

For comparison the total interaction probability and the probability for 2 or more interactions is shown. If the probability for a second interaction has to be negligible the thickness should stay below $0.5 x_0$ although the maximum for single interaction absorption has its maximum at x_0 . With $x_0 = 11.1 \text{ cm}$ for a plastic scintillator material a thickness of 2.2 cm would be a good choice resulting in an interaction probability of 18%. In addition the size of the first scintillator material defines the position of the first interaction and consequently the angular resolution of the measurement. Taking the other geometrical constraints into account a somewhat smaller value is chosen with a final efficiency of 9%. The scintillator is a rectangular prism of dimensions $12 \text{ mm} \times 12 \text{ mm} \times 40 \text{ mm}$ which is large enough to fully contain the electron ejected in the Compton process for most events. It is coupled to a photo-multiplier tube (Valvo XP 1911) and a μ -metal is used for the magnetic shielding. The whole system is placed in cylindrical aluminum tube which is fastened to a fixed position on the scattering platform defining the origin of the polar scattering geometry.

A Thallium doped Sodium iodine crystal (NaI(Tl)) is chosen for the second detector in order to provide a very good light output and at the same time a good absorption efficiency for the scattered photons (see fig.2 in the appendix B). The NaI(Tl) crystal still is the “working horse” in nuclear physics since it is easily available and has a reasonable decay time (230 ns) which is sufficient for fast coincidence measurement. The crystal has a cylindrical shape with a diameter of 2 inches and a length of 2 inches as well and it is hermetically sealed in an Al container because of its hygroscopic behavior. It is optically coupled to a XP2020 photo-multiplier tube, magnetically shielded with μ -metal and all the system including the resistive divider chain has been placed in a cylindrical Al shield. This detector is can be moved and locked at angular positions from -90 to $+90$ degrees in increments of 15 degrees.

Principle of Operation

The scintillators emit light in the visible wavelength range which is proportional to the amount of energy deposited in the material. Unfortunately the efficiency of this process is rather low and the statistical fluctuations of the emitted photons influence the time- and energy resolution of the measurement (for details see the lecture “Detectors”). Therefore very sensitive photo detectors have to be used. A single photon sensitivity is obtained with secondary electron multipliers coupled to a photo cathode. The assembly is housed in a highly evacuated glass tube and is consequently called photo multiplier. The principle of operation is shown in fig. 8. The photons emitted by the scintillator are send via light guides and carefully coupled using optical grease to a photo cathode where they produce a single electron via the photo effect with an efficiency of the order of 20%. For the generation of such photoelectrons in plastic scintillator an energy deposition of about 100 eV and in NaI(Tl) about 25 eV is required. These electrons are guided to the first dynode and accelerated at the same time by the electric field generated between the photo cathode and this electrode where they undergo multiplication via secondary electron emission. Since the focusing and accelerating properties at the first dynode are the most critical for the performance of the tube the voltage of this stage usually is independently accessible and can be externally adjusted. The following dynodes are connected to an increasing voltage (mostly realized by a resistor chain) and they multiply the number of arriving electrons further. For the total charge Q_0 collected at the anode it is obtained:

$$Q_0 = \eta N e_0 \quad \text{with } \eta \text{ the gain per stage and } n \text{ the number of stages.}$$

The factor η may range from 3..5 and therefore 10 to 14 stages are used in order to obtain enough charge at the anode to process the signal further in the electronics circuits. The gain of the whole dynode chain can be regulated by the total applied voltage to the resistor chain (see calibration in the next chapter).

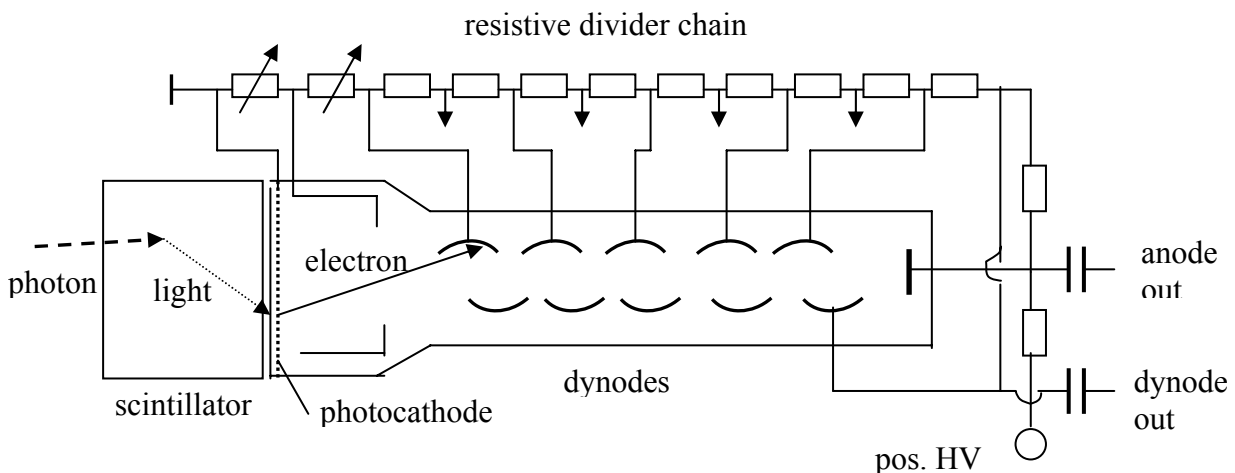


Fig. 8. Scintillator and photomultiplier

The setup used to perform the amplitude measurements (and thus the energy measurements) as function of the angular setting is shown in fig. 9. The signals from each photo multiplier is amplified and adapted in electronic circuits using mainly R-C- shaping stages (see lecture “measurements”). Each output signal is split. One branch is connected to the input of the digital oscilloscope for pulse height measurement and the other branch to the coincidence circuit. If a coincidence is registered the signal is used to trigger the oscilloscope. In this way only the selected

amplitudes are displayed and can be measured. The additional feature of the oscilloscope to perform an averaging of a pre-selected number of signals allows a more precise measurement despite the rather large fluctuations of single pulses.

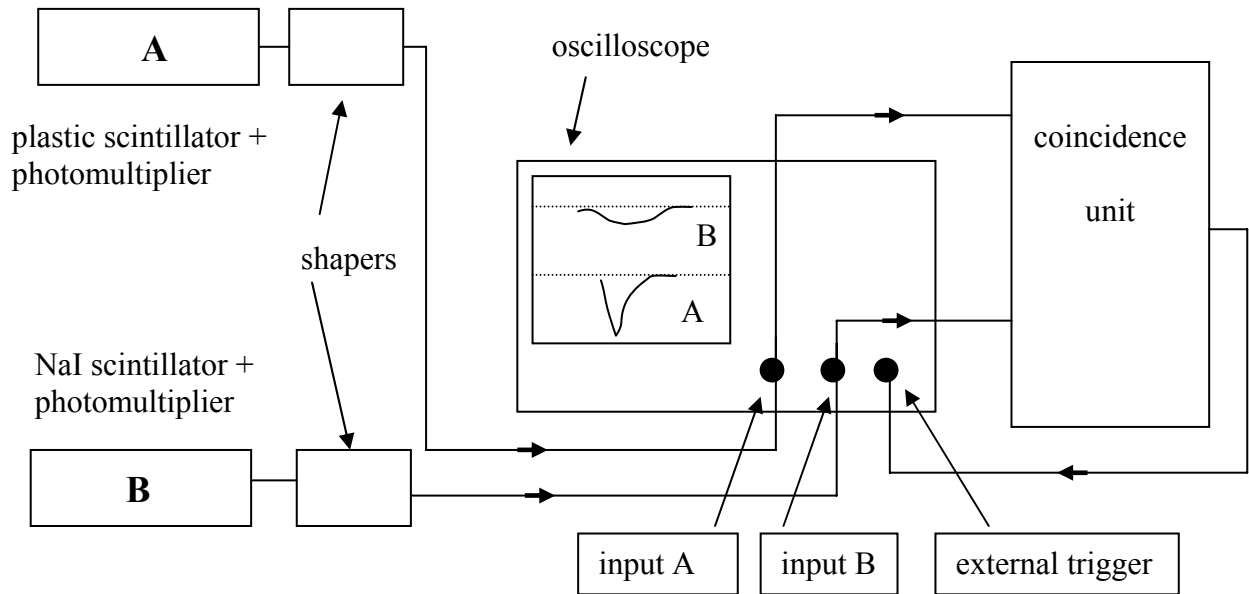


Fig. 9. Set-up for amplitude measurement with the oscilloscope

The coincidence circuit is shown in Fig. 10. It is noticed that the NaI branch splits again and is fed into two separate discriminator circuits, one at a low threshold in order to give a timing signal with the minimum jitter and a high threshold requiring a minimum amplitude to avoid small background signals. Since the low threshold is supposed to determine the timing it has to fall into a wide timing window of the high signal and therefore it is delayed. The first coincidence signal (coincidence I) provides a valid signal for the NaI detector. Consequently the signal from the discriminator of the plastic scintillator has to be delayed accordingly (see fig. 11 for timing diagram). Coincidences from both signals (coincidence II) define valid Compton events. The pin assignment for the shaper and discriminator circuit is shown in the Appendix B, fig. 3 and 4.

Sometimes the rates in each channel are very high and the coincidence signal representing the physics processes of interest are very rare. Therefore it is of interest to determine the probability of random coincidences n_{ran} . Using simple probability considerations one obtains:

$$n_{\text{ran}} = 2\tau n_A n_B$$

with τ the coincidence time resolution and n_a , n_B the rates of the channels A and B.

Therefore the coincidence time resolution is an important measure of a coincidence circuit and is kept as small as possible. In principle the coincidence time resolution is given by the sum of the width of both signals. This is due to the response of the electronic AND circuit (see for example data sheet of 74F08, Fig. 5 in Appendix B). Experimentally a possible jitter has to be taken into account. The measurement of the coincidence time resolution is performed by delaying one channel (here delay 1) and recording the count rate n_{coinc} in a scaler. For control purpose the individual

count rates n_A and n_B are recorded as well. The relative adjustment of the timing for the signals is shown in fig. 11.

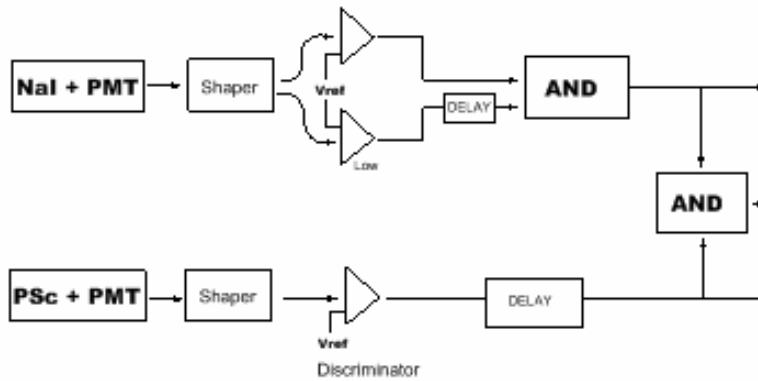


Fig. 10 coincidence circuit

In the ideal case, the energy of the gamma rays emitted from the source would produce a very sharp peak in the energy spectrum. However, due to noise and statistical fluctuations, this is not the case in practice. The better the resolution of the detector is, the narrower this peak becomes. Resolution

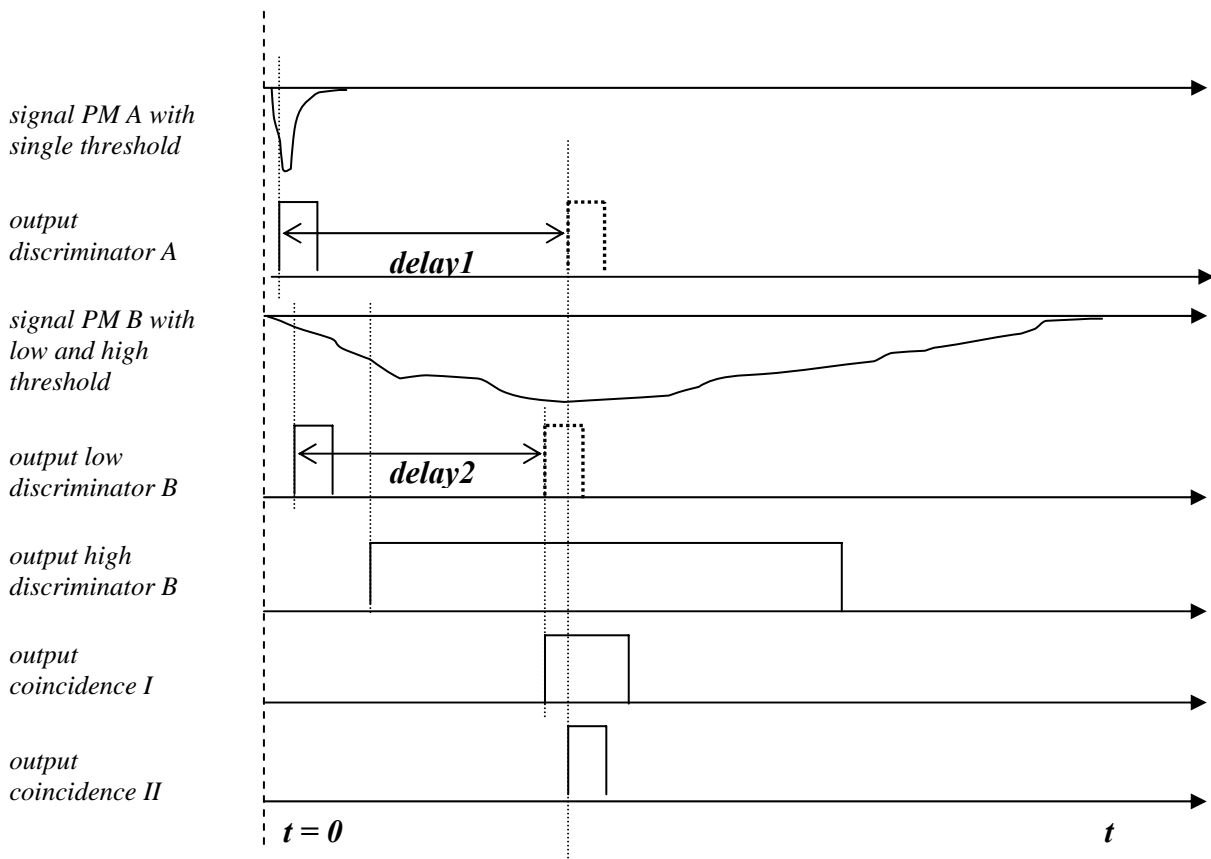


Fig. 11. Timing diagram of the coincidence circuit

ΔE is usually expressed in terms of the full width of the peak at half maximum(FWHM) or the percentage of the full width at half maximum which is defined as $\Delta E/E \times 100$. The plastic detector used for this experiment has an energy resolution of the order of 13-15 % and the NaI detector around 9 %.

When a gamma ray of energy E_γ hits the detector and all its energy is collected, a voltage pulse occurs corresponding to this energy. However, not always the collection of the full energy is possible and this results in more peaks in the spectrum. Depending on the destiny of the photon within the detector, besides the photo-absorption peak, the Compton continuum, the backscatter peak, escape peak and sum peak are also observed. The mean energy values corresponding to these peaks for a certain source are known both experimentally and theoretically and they are used to perform the energy calibration. For the mono energetic ^{137}Cs source used here the Compton edge is used for calibration of the plastic detector and the photo peak for the NAI detector. The pulse height distribution can be estimate with sufficient precision from the oscilloscope in the single event sampling mode. Since the threshold for timing has to be as low as possible the calibration is carried out as function of the high voltage in order to determine the optimum operation voltage.

Experimental Procedure

The main tasks comprise:

- Calibration of detectors
- adjustment of coincidence circuits
- energy measurements as function of scattering angle

1. Energy Calibration

Start with plastic scintillator detector by attaching the source (with tape) to it.

Apply +800V to the detector.(WARNING: INCREASE HIGH VOLTAGE SLOWLY (100V/sec max). The high voltage is adjusted with a HELIPOT with 10 turns. One turn= 1.0 SU (scale units) corresponds to 200 V, thus +800V are 4.0 scale units.

Set the digital scope acquisition mode to single sampling mode and note the maximum pulse height Repeat this procedure up to +1200V (6.0 SU). A logarithmic plot of the measured pulse height as function of the high voltage allows a linear fit which can be used by applying a multiplication factor to obtain the calibration curves for other energies. These calibration lines are used to verify that the threshold of 30 keV which is needed for recording the Compton electron at small scattering angles can be reached at the highest allowed voltage for the smallest stable threshold of 6 mV.

Repeat the upper procedure for NaI detector. But for this case the high voltage should be in the range of -1400V to -1800V with 50V steps (negative high voltage!). Note that the photo peak and the Compton edge are visible. The photo peak is well pronounced and easier to use. An example of such a measurement is shown in fig. 12. As explained above, the signal amplitude is taken from the output of the shaper. In order not to disturb the same signal for the discriminator (a twisted pair cable is used with an impedance matched to the input of the discriminator in order to avoid reflections) the signal is picked up by a small divider circuit as shown in fig. 13. Therefore the measured amplitude on the oscilloscope has to be multiplied by the factor 20. The same "probe" is used to connect the digital output of the logic circuits to the oscilloscope.

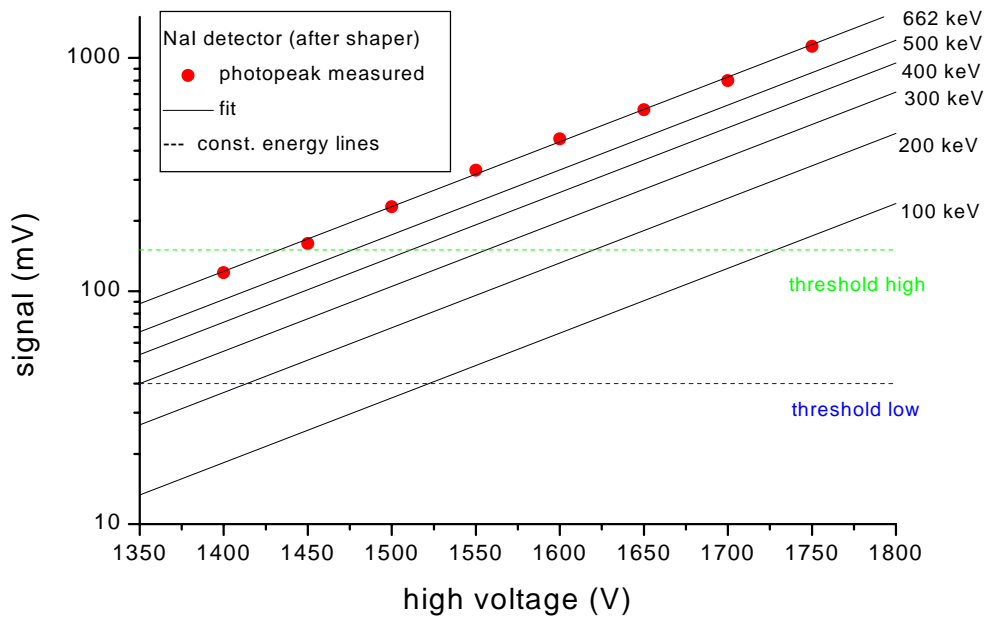


Fig. 12. Energy calibration of the NaI detector.

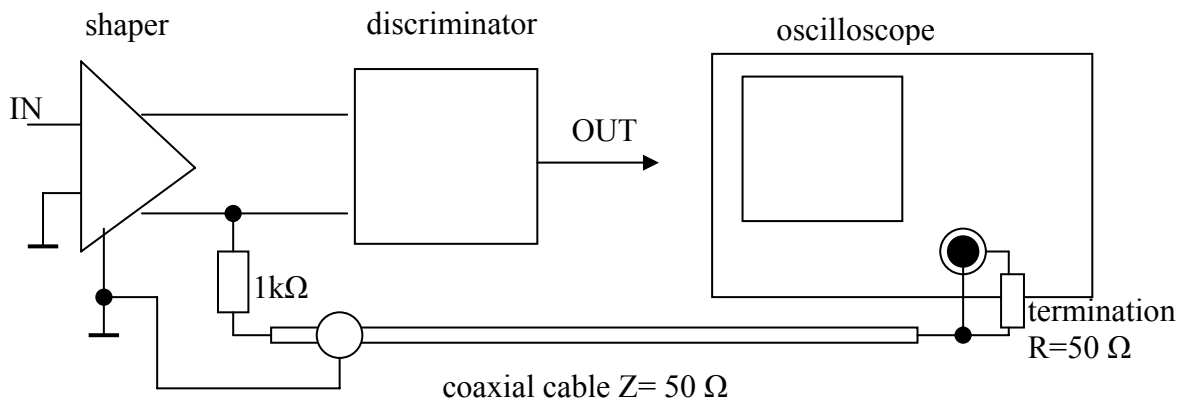


Fig. 13. Schematics of a probe for signal pick-up from the circuit board

2. Coincidence measurements.

Leave the source on the plastic scintillator and reduce distance between the plastic scintillator and the NaI (about 10 cm) in order to maximize the rate. The height of the NaI detector should be such that the axis of the beam intersects its mid-plane.

Apply previously determined voltages to the photo multipliers.

Adjust delay 2 to a value of 350 ns by trimming the value of the resistor in the corresponding timing circuit. Pin 6 and 7 of the retriggerable one-shot (for example 74LS123, fig. 6 in the appendix) are bridged by C and R connects to pin 7 to V_{cc} . Check signals from scintillators on the oscilloscope before starting the coincidence measurement and record the count rate for each detector without source.

In order to separate random coincidences from the real ones, a coincidence curve should be plotted. Record the coincidence counts for 60 sec. by applying different delay values delay1 to the signal of the 1st detector. Plot the result and after analyzing the resulting coincidence curve, fix the delay at the most appropriate setting.

3. Compton coincidence measurements

The source is now placed behind the support of the first detector and the lead collimator consisting of two parallel lead plates. Position NaI detector at about 20 cm from the scattering center. Set the scope to averaging mode with 16 samples and measure energy in the detectors.

Repeat the procedure up to 90° in steps of 15° .

By using the Compton formula, calculate the theoretical values for the scattered electron and photon energies. Then compare these results with the experimental values.

Appendix A: Derivation of the Compton Formula

Consider the Compton interaction (Fig. 1) between a photon with energy E_γ and an electron initially at rest with rest mass m_e . The initial and final photon momenta are denoted by the unit vectors \vec{a} and \vec{a}' respectively. The recoil electron has an energy E and momentum \vec{p} .

By conservation of energy:

$$E_\gamma + m_e c^2 = E' + E$$

and by conservation of momentum

$$\frac{E_\gamma}{c} \vec{a} = \frac{E'}{c} \vec{a}' + \vec{p}$$

Simple manipulations lead to the following equations:

$$(E_\gamma - E') + m_e c^2 = E$$

$$E_\gamma \vec{a} - E' \vec{a}' = \vec{p} c$$

Taking the square of both and performing the subtraction gives Poincaré's invariant mass $m_e^2 c^4$:

$$2E_\gamma E' (1 - \cos \theta) - 2(E_\gamma - E') m_e c^2 + m_e^2 c^4 = m_e^2 c^4$$

$$\Rightarrow (E_\gamma - E') m_e c^2 = E_\gamma E' (1 - \cos \theta)$$

and finally the Compton scattering formula:

$$E' = E_\gamma \frac{1}{1 + \alpha(1 - \cos \theta)} \quad \text{with } \alpha = E_\gamma / m_e c^2$$

and for the electron energy:

$$E = E_\gamma \frac{\alpha(1 - \cos \theta)}{1 + \alpha(1 - \cos \theta)}$$

Appendix B. Useful data

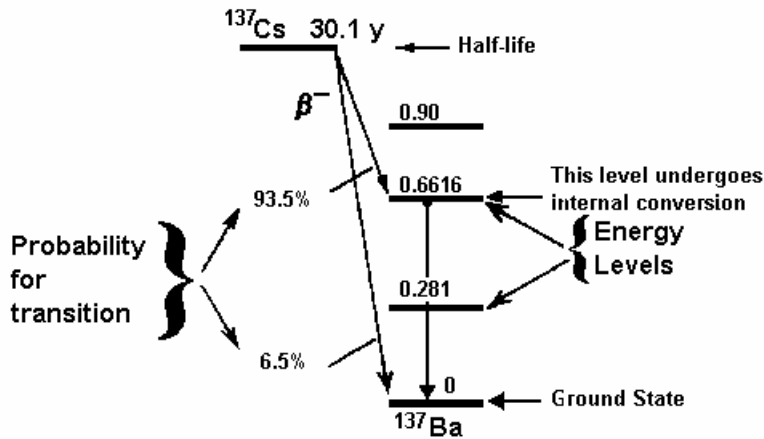


Fig.1 Decay schematics of ^{137}Cs .

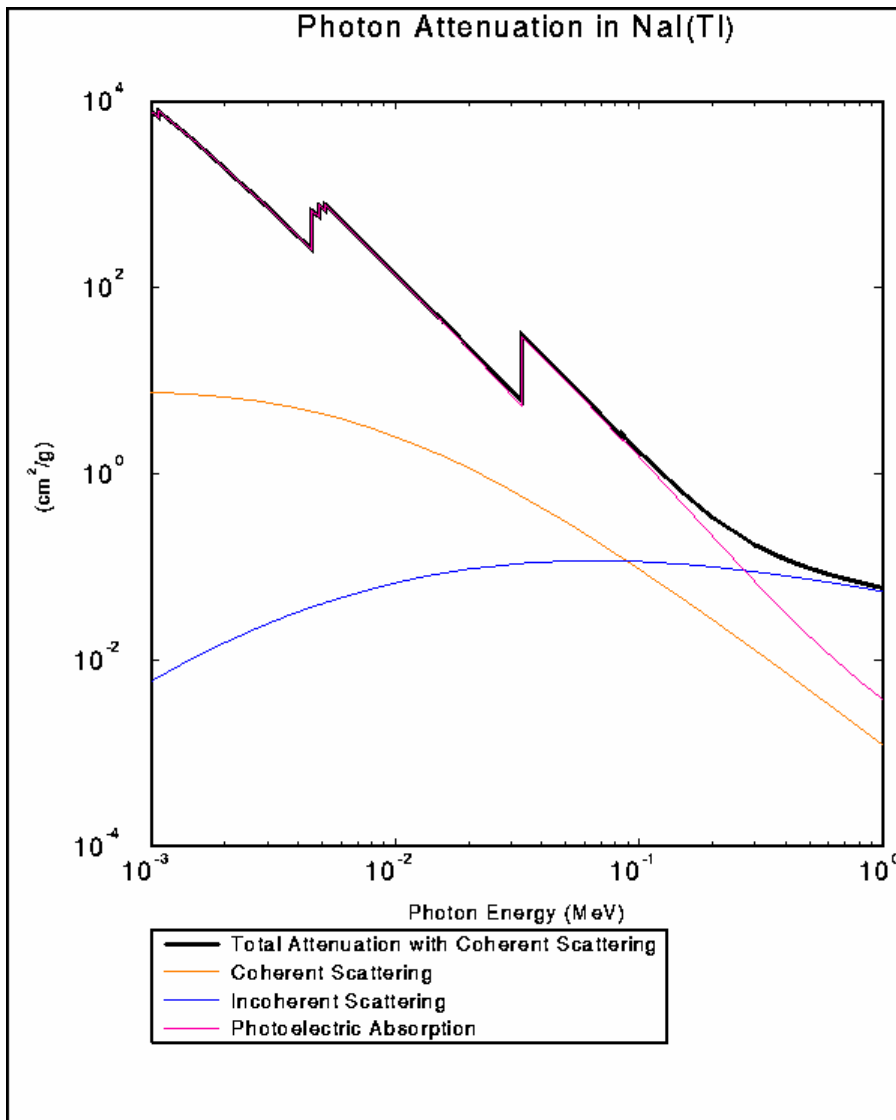


Fig. 2 Cross-sections of sodium iodide with 1.7% Tl by weight showing total absorption and fractional components due to Compton scattering, photoelectric absorption and incoherent scattering. Data are from the NIST XCOM Database (see references below).

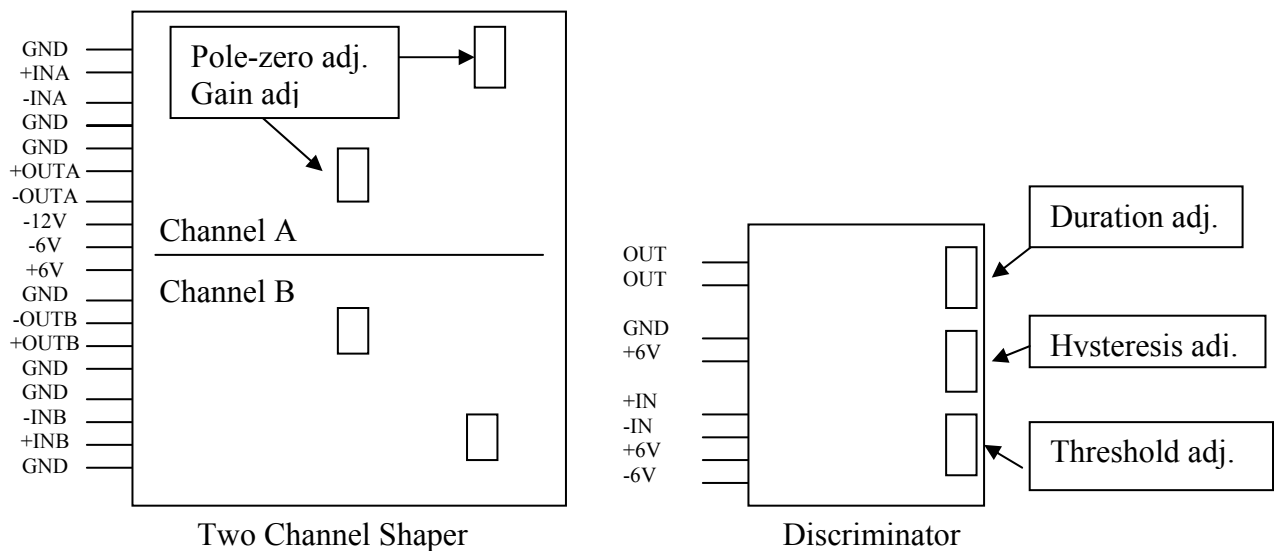


Fig. 3,4. Pin assignment of the shaper and discriminator circuits

Fig. 5,6 Data sheets for AND gatter and one-shot (see below).

Additional Textbooks and References

"Particle Detectors", C.Grupen, Cambridge Monographs on Particle Physics, Nuclear Physics and Cosmology, 1996.
 "Techniques for Nuclear and Particle Physics Experiments: A How-to Approach", W.R.Leo, Springer Verlag, Second Revised Edition, 1994.
 "Classical Electrodynamics", J.D.Jackson, 2nd Ed. New York:Wiley, 1974.
 "Compton Scattering", MIT Physics Laboratory Experiment, 1, 2000.
 "Compton Scattering", University of California at Berkeley Physics 111 Laboratory, 2000.
 "The Gamma Counting Handbook", EGG Wallac,
 "Table of Nuclides", <http://www.dne.bnl.gov/CoN/index.html>.
 "NIST Physical Reference Data", <http://physics.nist.gov/PhysRefData/contents.html>.